Our Project: Quarternion Joint

Harris Ramos Baroni, Hassan Shazad, Benjamin Li[a]

[a]*Department of Computer Science, University College London,*

1. Introduction

The development of strong, agile and safe humanoid robot mechanisms remains a fundamental trilemma to the field of robotics. A step towards this harmony is found in the research of Yong-Jae Kim, Jong-In Kim, and Wooseok Jang from Naver Labs. They developed LIMS2-AMBIDEX (LIMS2), a revolutionary device involving a 3-DOF wrist mechanism, which we have taken inspiration from for our 1st term undergraduate project. Expect our mathematical notation to be consistent with theirs.

LIMS2 is tendon-driven and achieves a spherical pure rolling motion in a confined central space, made possible by a unique parallel link mechanism. The simple, compact and reliable structure of this parallel mechanism enables fast, accurate and high payload actuation [5].

Despite being outdated by an improved LIMS3-AMBIDEX, a lack of academic papers meant we proceeded learning from LIMS2, still a revolutionary contraption. An ability for uniform manipulation and a large range of motion, while maintaining stiffness and strength, is the reason this wrist mechanism is so significant. Safety was also improved by making the mechanism wire-driven, meaning mass and inertia could be reduced and backdrivability increased [5]. Mechanisms such as this will replace tedious or dangerous work in the future, utilising human tools and workspaces. Its unique design and improved capabilities will make it suitable for a wide range of applications, which is why our team took interest in this design. Applications include industrial automation, medical robotics, and space exploration.

Similar developed mechanisms struggle to reconcile safety and effectiveness. For example, the KUKA-DLR Lightweight Robot arm, despite having a low mass-payload ratio and a programmable, active compliance [1], force and torque sensors to ensure safety prove unreliable at high speeds. Moreover, mechanisms using various series elastic actuators (SEAs) [2] and variable

stiffness joints (VSJs) [6] trade a high compliance with reduced accuracy due to low joint stiffness.

Looking elsewhere, Project Blue, developed by University of California, Berkeley is an example of a low-cost, compliant robot capable of basic manipulation tasks via a quasi-direct drive. However, it is at the expense of a reduced max load at continuous operation and a relatively low bandwidth for industrial standards. Admittedly, their design focused on being cost-efficient and for household tasks, contrary to LIMS2, developed for more industrial purposes [3].

Wire-driven mechanisms, where for LIMS2 the motion of the wires directly represents the quaternion motion of the joint, are known to have a poor control performance owing to a low stiffness of the tendons. Therefore, while developing LIMS1-AMBIDEX (LIMS1), novel tension amplification mechanisms had to be introduced [4]. However, LIMS1 involved a complex mechanism that had a low payload and stiffness. The development of LIMS2 attempted to solve this, proposing an extremely simple and compact structure whilst improving all specifications.

In this project, we aim to examine the assembly and range of motion of the mechanism. Additionally, we will verify the mechanism's ability to approximate the ideal circular rolling motion with acceptable accuracy.

2. Mathematical modelling

2.1. Basic 2D Model

The joint's kinematic structure is derived from the basic 2-dimensional (2D) model shown in figure 1. It is a pure rolling joint as its motion is equivalent to two ellipses rolling on each other without sliding. This is thanks to the clever arrangement of linkages as an anti-parallelogram, which is characterised by AC being parallel to BD (figure 1). The crossing point of links AD and BC is the point F, which represents the point of contact between the two rolling ellipses, as shown in figure 2a.

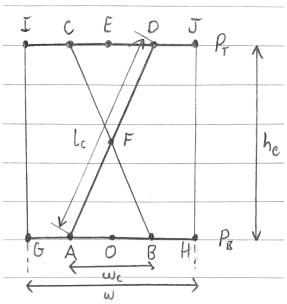

Figure 1: 2D mechanism in resting position

The bottom plate P_B and top plate P_T both have length w while AB and CD have length w_c. P_B and P_T are connected by the two links AD and BC of length l_c. The links AD and BC have hinge joints on both their ends. They are not joined at F. Define α as the angle between the normals of P_B and P_T, and call it the bending angle. The bending plane is the plane which contains the normals of P_B and P_T (which in 2D is just *the* plane). It is useful to set the centre O of P_B as the origin. If θ is the polar angle of OE then $\alpha = 2\theta$. Cables of length l_{p1} and l_{p2} connect G, I and H, J respectively. These cables are set to length $h_c = \sqrt{l_c^2 - w_c^2}$ when $\alpha = 0$, which we will call its rest pose. The wrist is tendon-driven: the cable lengths dictate the pitch of the joint, hence the subscript p.

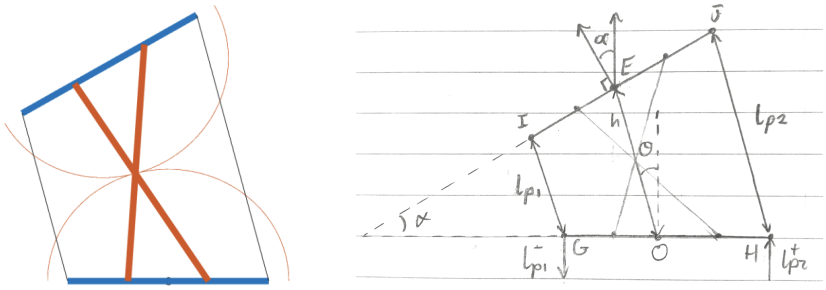

(a) Motion mimics rolling ellipses (b) 2D model of antiparallelogram linkage during tilt

Figure 2

If we fix P_B and vary α, then P_T rolls around the crossing point F of AD and BC. During this motion, we see the lengths l_{r1} and l_{r2} vary in figure 2b but $AF + BF = l_c = constant$ as shown in figure 2a. By the definition of an ellipse, this tells us that F follows an elliptical path with foci at A and B. Draw a tangent to the ellipse at F. Due to symmetry along this tangent, we can determine that C and D are the foci of an identical ellipse and thus we have shown that the mechanism does indeed describe the rolling motion between two ellipses.

Since the angle α is fully determined by the lengths l_{p1} and l_{p2} provided all the links lengths are established, it is beneficial for us to find this rela-

tionship. This is to determine the displacement of the linear actuation wires represented by l_{p1} and l_{p2} required to change angle α.

Noting that a projection of w onto OE is given by $w \sin\theta$, it is clear that the equation that relates the lengths of the two cables is:

$$l_{p1} = l_{p2} - 2w \sin\theta \tag{1}$$

Then substituting in $l_c^2 = l_{p1} l_{p2} + w_c^2$ (Ptolemy's Theorem for isosceles trapezoids) and solving a quadratic, we obtain:

$$l_{pi}(\theta) = \sqrt{l_c^2 - w_c^2 \cos^2\theta} \pm w \sin\theta. \tag{2}$$

Finally, use $\theta = \frac{\alpha}{2}$ to obtain

$$l_{pi}(\alpha) = \sqrt{l_c^2 - w_c^2 \cos^2(\tfrac{\alpha}{2})} \pm w \sin(\tfrac{\alpha}{2}). \tag{3}$$

We won't shy away from using eq. (2) instead of (3), though. We can express the geometry of our mechanism is a more concise and natural way using the polar angle rather than the bending angle.

2.2. Basic 3D model

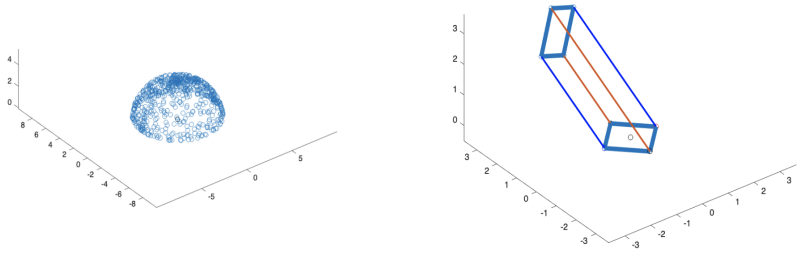

(a) Locus of F forms an oblate ellipsoid (b) Cable pairs dictate roll and pitch

The range of motion of the point F in the 3D model is shown in figure 3a. Let us describe the oblate ellipsoid spanned by F as the wrist moves. It has centre O, extends out by length $\frac{l}{2}$ in the x and y directions and by length $\frac{h_0}{2}$ in the z direction. Using spherical coordinates $(x, y, z) \rightarrow (r\sin\theta\cos\phi, r\sin\theta\sin\phi, r\cos\theta)$, the oblate ellipsoid is described by:

$$\left(\frac{r\sin\theta\cos\phi}{l_c/2}\right)^2 + \left(\frac{r\sin\theta\sin\phi}{l_c/2}\right)^2 + \left(\frac{r\cos\theta}{h_c/2}\right)^2 = 1 \tag{4}$$

Rearranging for r, we obtain:

$$r(\theta) = \frac{l_c h_c}{2\sqrt{(h_c \sin\theta)^2 + (l_c \cos\theta)^2}} \tag{5}$$

Equation (5) makes it clear that, for an oblate ellipsoid, the radial length from the centre to the surface is impacted only by the polar angle θ and not the azimuthal angle ϕ. Instead, ϕ determines the plane in which the wrist bends: the bending plane. The cross section of the oblate ellipsoid is the same in any bending plane: they are all equivalent ellipse shapes. Thus, any further assertions made about the ellipse spanned by F in the 2D case applies to a cross section of the ellipsoid spanned by F in the 3D case. Therefore, just as in the 2D case, the bending angle is equal to 2θ.

Introduce another pair of cables of length l_{r1} and l_{r2} which determine the roll of the joint, hence the subscript r. Using similar geometrical arguments used to obtain eq.s (1) and (2) and the fact that θ is half of the bending angle, we can derive the following equations:

$$l_{pi}(\theta, \phi) = h(\theta, \psi) \pm w \cos\phi \sin\theta \tag{6}$$

$$l_{ri}(\theta, \phi) = h(\theta, \psi) \pm w \sin\phi \sin\theta \tag{7}$$

where $h(\theta, \psi)$ is some function describing the distance OE, akin to the first term of eq. (2). Intuitively, $w \cos\phi$ is a projection of w onto the bending plane when w is in the plane between the cables determining pitch. Since the cables that determine roll are at right angles to the cables that determine pitch, the factor for their projection onto the bending plane is given by $\cos(\phi \pm \frac{\tau}{4}) = \mp \sin\phi$ (where $\tau = 2\pi$). One final projection onto the line OE is given by the factor of $\sin\theta$.

2.3. Approximating a circular pure rolling joint

Recall eq.s (1), (2) and refer to figure 2b. We can also use geometry to show that $h = l_{pi} \pm w \sin\theta$ and therefore $h = \sqrt{l_c^2 - w_c^2 \cos^2\theta}$. Thus h is not a constant. Let us briefly investigate the implications of having a constant h. Let (l_{p1}^+, l_{p2}^-) denote the displacements in the cable pair dictating pitch and suppose that h is some constant k. Then eq. (2) becomes

$$l_{pi} = k \pm w \sin(\tfrac{\alpha}{2}) \tag{8}$$

which tells us that the change in lengths of the cables as α varies is equal and opposite: $l_{p1}^+ = -l_{p2}^-$. We could use the same mechanism that adds length to

l_{p1} to subtract length from l_{p2}. Yong-Jae Kim, Jong-In Kim, and Wooseok Jang argue that it is useful for the elliptical motion to be as close to pure spherical rolling as possible [5]. Indeed, if this were achieved, our h would be approximately constant and the proposed mechanism could be implemented. We will do this in the 2D case, but the results extend directly to 3D.

Firstly, we know that A, B and C, D are the foci of the ellipses. A circle is a special case of an ellipse were the foci are on top of each other. Reducing the distance $w_c = AB = CD$ between the foci and increasing the length $l_c = AD = BC$ has the effect of bringing the foci of each ellipse closer (relative to the ellipse's dimensions). This makes the elliptical motion closer to that of a circle.

To take things further, we can find which osculating circles approximate the ellipse that is the locus of F. The radius of curvature R of a curve at the point with coordinates (x, y) is given by

$$R = \frac{x'^2 - y'^2}{x'y'' - y'x''}. \tag{9}$$

Parameterising the ellipse using $(x, y) \rightarrow (\frac{l_c \sin\psi}{2}, \frac{h_c \cos\psi}{2})$ and calculating derivatives with respect to ψ, we obtain the following equation:

$$R = \frac{(l_c^2 \cos^2\psi + h_c^2 \sin^2\psi)^{\frac{3}{2}}}{2 l_c h_c}. \tag{10}$$

R evaluated at a given ψ gives us the best *local* circle approximation, but we seek an approximation of the ellipse over a whole range of ψ. We can find the mean value of R within a desired range of ψ and this can describe in some way the best circle to approximate the ellipse within that range:

$$R_{mean} = \frac{1}{\psi_2 - \psi_1} \int_{\psi_1}^{\psi_2} R d\psi. \tag{11}$$

Place the circle with radius R_{mean} so that it is $h_0 = R_{mean} - \frac{h_c}{2}$ below the centre of the ellipse. Note that R is symmetrical along ψ=0. If we integrate over the range $[0, \frac{\tau}{8}]$ and set l_c=86mm and w_c=30mm then R_{mean}=44.375mm and h_0=4.076mm. Using eq. (14), we find that the circle with radius R_{mean} differs from the ellipse by at most 0.184mm within our range. So if we offset the links from P_B and P_T by h_0, then the ellipse drawn by F is approximately the same as a circle of radius R_{mean} with its centre in the middle of P_B.

This is sufficient for the purpose of constructing a 2-DOF basic mechanism (considering the fact that it is not affected by backlash), but higher precision may be necessary for our 3-DOF mechanism which features a non-compliant shaft connecting OE.

In our tests, the most successful method to find a circle which best describes the ellipse is the following. We first suppose that there is some circle with radius R whose centre is h_0 below the centre of the ellipse that best fits its curve. Take the centre of this circle to be the point with coordinates $(0, 0)$. Then the equation describing the ellipse is:

$$\left(\frac{x}{l_c/2}\right)^2 + \left(\frac{y - h_0}{h_c/2}\right)^2 = 1 \tag{12}$$

Using polar coordinates $(x, y) \to (\rho \sin\psi, \rho\cos\psi)$ and then rearranging for h_0, we obtain

$$h_0(\psi) = \frac{2l_c\rho\cos\psi - h_c\sqrt{l_c^2 - 4\rho^2\sin^2\psi}}{2l_c} \tag{13}$$

Rearranging eq. (13) instead for ρ:

$$\rho(\psi) = \frac{2l_c^2 h_0\cos\psi + l_c h_c\sqrt{l_c^2\cos^2\psi + (h_c^2 - 4h_0^2)\sin^2\psi}}{2(h_c^2\sin^2\psi + l_c^2\cos^2\psi)} \tag{14}$$

Fix ρ to some chosen value. Now carefully compare the coefficient of ρ in eq. (13) to the coefficient of a fixed h_0 in eq. (14). We see that the relationship ψ and ρ nearly mirrors that of ψ and h_0. This is evident in figure 4b. With this, we can now propose some sort of measure which describes how much each one deviates from a fixed value as ψ varies in the range $[0, \frac{\tau}{8}]$. Since variations in $h_0(\psi)$ mirror variations in $\rho(\psi)$ we will choose to measure using $h_0(\psi)$ as eq. (13) is friendlier. In our testing, it is sufficient to measure this variation using a single difference: $deviation = |h_0(\frac{\tau}{8}) - h_0(0)|$. Let ρ_{min} have the value which minimises this deviation, i.e, makes the deviation equal to 0. Then it is given by

$$\rho_{min} = \frac{(2-\sqrt{2})l_c^2 h_c}{(3-2\sqrt{2})l_c^2 + h_c^2}. \tag{15}$$

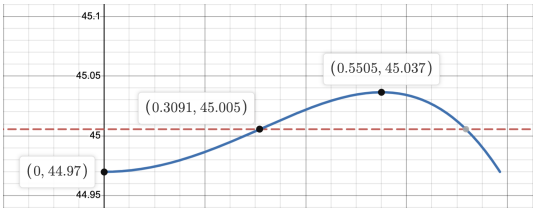

(a) ρ against ψ

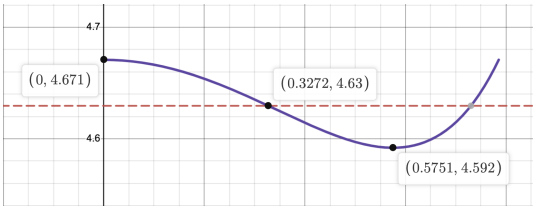

(b) h_0 against ψ

Figure 4: Dotted lines represent mean values of the functions

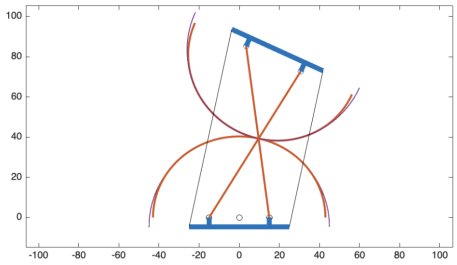

Figure 5: Purple circles are approximated by the orange ellipses

Now, we choose the value of h_0 when $\psi = 0$ (or $\frac{\tau}{8}$) and $\rho = \rho_{min}$[1] to serve as the displacement of the ellipse's centre. Figure 4a shows the variation of $\rho(\psi)$ when l_c=86mm and w_c=30mm so that ρ_{min}=44.97mm and h_0=4.671mm. We see that $\rho(\psi)$ remains more or less constant, deviating from its mean value 45.005mm by at most $\pm$0.035mm. So we can say that $\rho(\psi)$ approximates the circle with radius R=45mm with reasonable accuracy. Recall that the assertions made in this section extend equivalently to 3 dimensions[2]. So, we can settle with this degree of accuracy as it is sufficient for our purposes of constructing the 3-DOF joint.

We can now assert within reason that the $h(\phi, \theta)$ of eq.s (6) and (7) is constant. Thus the extension of eq. (8) to 3 dimensions is

$$l_{p1}^{+} = -l_{p2}^{-} = w \cos\phi \sin\theta \quad \text{and} \quad l_{r1}^{+} = -l_{r2}^{-} = w \sin\phi \sin\theta. \tag{16}$$

[1]Indeed, due to the symmetry between eq.s (15) and (16), this value of h_0 actually minimises $|\rho(\frac{\tau}{8}) - \rho(0)|$. The exact solution to this is ungodly, so we choose to spare the reader from it's sight. (It's monstrous.)

[2]One would find that the radial length ρ from the origin to an oblate ellipsoid whose centre has Cartesian coordinates $(0, 0, h_0)$ is independent of the azimuthal angle when describing the problem in spherical coordinates.

This is very useful: define the *scaled cable displacements* for pitch and roll $p \equiv \cos\phi \sin\theta, r \equiv \sin\phi \sin\theta$ respectively. Here is a pleasant result

$$\sin\theta = \sqrt{p^2 + r^2} \quad \text{and} \quad \sin\phi = \frac{r}{\sqrt{p^2 + r^2}}. \tag{17}$$

3. Mechanical analysis

3.1. 3-DOF model

Figure 6: 3-DOF mechanism

We will now describe the mechanism show in figure 6. This mechanism features 3 parallel links connecting the top and bottom plates which approximate the antiparallelogram mechanism of figure 1 in any bending plane. Their centres of rotation are offset by some h_0 from the very top and bottom plates thus approximating the rolling motion of two spheres of radius ρ_c. Unfortunately, we are not at a stage where we can verify by ourselves that this mechanism approximates this ideal spherical rolling motion with acceptable accuracy. For a full assessment of the mobility of a 3 link mechanism, see [5].

Spheres are sandwiched between a plate and a flat panel called a brace. These spheres freely rotate between the plate and brace so they act as the ball joints at either end of the links. The 3 links are connected to the plates every 120° and their structures are designed to leave a cavity for a central shaft. Two pairs of opposite cables are fixed to the top plate and feed through the bottom plate. Each pair dictates the pitch and the roll respectively through pulley systems.

A hand freely rotates at the top, but is not powered by any transmission system. A later prototype would ideally include a central shaft which uses a universal joint at the top and bottom to power this distal yaw motion. It may include a gear reducer (e.g. planetary gear) at the top. So, this proposed mechanism has a further degree of freedom.

3.2. Pulley system

Since this quaternion joint mimics spherical rolling, the change of length in the opposite cables are equal and opposite. We can use a pulley system

where the cables are of constant length and thus constant tension to implement these changes in lengths. A simple example is shown in figure 7a, which is sufficient for manual driving of the roll and pitch cables. The pulley system for the yaw motion allows for motor actuation. The choice to use cables over, say, a bevel gear for the yaw motion is because it is mechanically simpler and does not suffer from backlash. For the pitch and roll cables to avoid intersection and causing friction, the radii of the pulleys for each cable must be different.

A more complex design for actuation of either roll or pitch cables is shown in figure 7b, which is more appropriate for implementation of motor actuation or incorporation into a full robot arm. This mechanism can be duplicated so that the pitch and roll cables can be driven in parallel, which replaces the crossed roll and pitch cables from 7a.

Our actual implementation of the pulley system shown in fig. 8b uses the simpler design. The bottom plate of the base has four sections which extend out and contain holes to guide the cables through to the pulley system. These holes act as the bending points of the cables during motion of the wrist so they are vertically offset by nearly the ideal h_0 from the centres of rotation of the parallel links (the centres of the spheres). This implementation is not optimal, but the effect of these errors is mitigated through a spring suspension mechanism between the pulleys and the wrist.

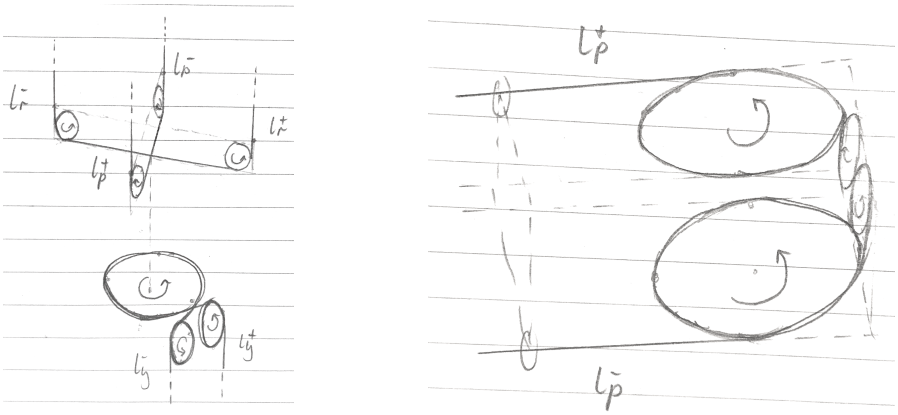

(a) Simple roll, pitch and yaw pulley system

(b) A more complex design for actuation of pitch or roll cables

Figure 7: Arrows show direction of travel of cables

3.3. Ball joints and motion analysis

Our particular implementation of the ball joints includes a peculiarity which turned out to be our largest oversight: our parallel links each have an unwanted third degree of freedom. Define the *articulation axis* of a parallel link as the line segment connecting the centres of spheres at either end of the link. Then each parallel link can *swivel* around its articulation axis. This allows the top of the wrist to produce an unwanted yaw motion, but this effect is substantially mitigated by increasing tension in the cables. If we ignore this effect, then the swivelling of the links does not impact the *geometry* of the wrist's motion (the wrist still satisfies spherical rolling) since each articulation axis remains invariant under a swivel, but it can impact the *range* of motion as the links can physically interfere with each other due to their shapes.

Observe the section of the parallel links which extends vertically out of the ball joints in fig. 8a. These all remain parallel if we once again ignore the yaw motion of the top of the wrist. Thus, the limit of bending in any direction occurs when these sections strike the braces. Our latest prototype reduces the dimension of these sections and we chamfered the holes in the braces to vastly extend this limit, resulting in $\pm 80^\circ$ range of motion in any bending plane whenever swivelling of the links does not restrict it.

3.4. Summary

The mechanism in figure 6 contains

- 3 parallel links
- 6 ball joints
- It has 3 degrees of freedom.
- The bending angle has a range of motion of $\pm 80^\circ$ in any bending plane.
- It uses a pulley system to enable the mechanism's roll, pitch and (ideally) yaw motion.
- The dimensions of the 3 parallel links and their offset the plates satisfy the restrictions which keep eq.s (13), (14) and (15) in the real domain.

4. Computer Design

Here is a collection of CAD designs and renders of our mechanism.

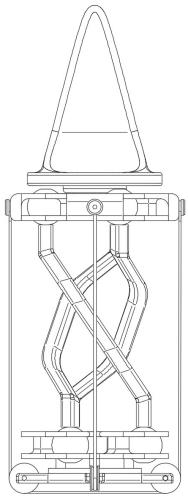

(a) Schematics of 3-DOF model

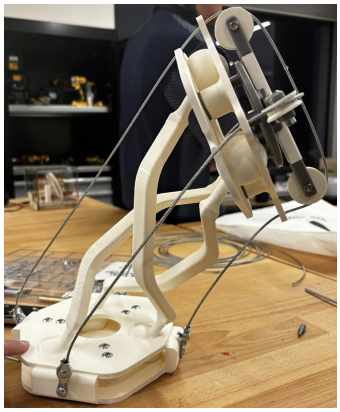

(b) Assembled wrist in a bent pose

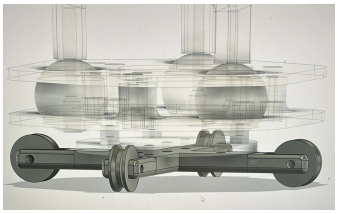

(c) Pulley system CAD

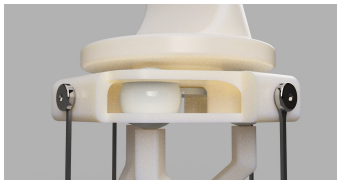

(d) Ball joints sandwich design

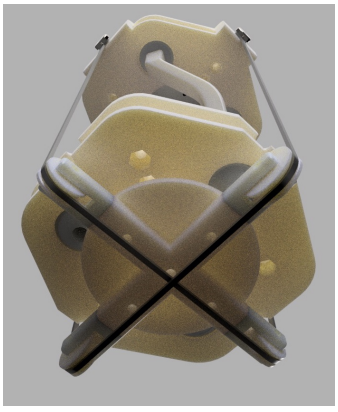

(e) Render of pulley system

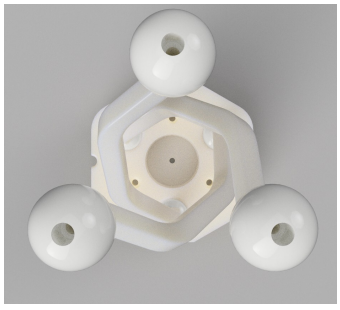

(f) Render of cavity for central shaft

Figure 8

5. Assembly

Here is an outline of how the mechanism in fig. 6 was assembled, starting from the bottom and working upwards.

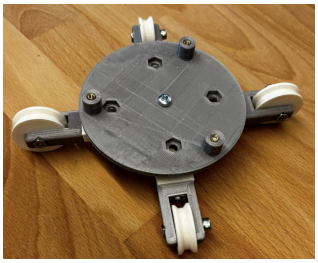

(a)

(b)

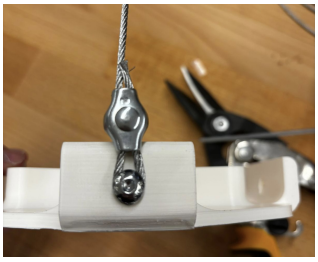

(c)

Figure 9

1. Assemble the pulleys into the frame as shown in fig. 9a and secure using screws.
2. Screw the pulley system frame into the bottom plate.
3. Place spheres on one side of a brace. Screw the links into the spheres through this brace.
4. Sandwich these 3 spheres between the bottom plate and brace. Secure the plate and brace together with screws, as shown in fig. 9b.
5. Sandwich the remaining 3 spheres as well as well as the disk between the top plate and brace. Secure with screws.
6. Screw these upper spheres into the links to connect the top and bottom sections.
7. Measure out appropriate cable lengths (we used steel rope wire). Bend and crimp cables into a loop. Screw through loop into the top plate as shown in fig. 9c. Feed the loose end through the guides and pulley system then bend, crimp and screw to the opposite side. This is, say, the pitch cable. Repeat for the roll cable.
8. Screw the hand to the disk in the top plate.

Thanks to the modular design of our mechanism, many of the steps outlined above may be taken in a different sequence. It also facilitates maintenance as parts can be swapped out without having to disassemble the entire mechanism.

6. Discussion and Conclusion

Overall, we believe that our quaternion joint project has been very successful relative to our own standards.

We were pleased to independently describe how to approximate spherical motion in the joint (which arguably improves on the method used in [5] in the 2D case). This elegantly led to the derivation of equations which describe the forward and inverse kinematics (eq.s (16) and (17)). A solid understanding of the geometry of the wrists motion enabled freedom for a creative design and allowed us to make educated decisions and suitable adjustments.

We were most impressed by our modular design: the components can be easily swapped out to make suitable adjustments. This came in very useful such as when one of our parallel link prototypes caused restricted motion due to its dimensions and we replaced it with a more refined design. Other components were made adjustable so that we may tighten connections or adjust tension in the cables in order to fine-tune the mobility of the wrist.

Aside from our important discussion in mechanical analysis section 3.3, we were very satisfied with our ball and socket linkage due to its design efficiency, incorporating a design whereby the spheres are sandwiched between plates and braces. This sets it apart from other designs while demonstrating that both universal and ball joints can be suitable for the parallel links of the wrist. In the future, however, we would try to restrict the extra degree of freedom which we did not account for, perhaps by taking inspiration from the mechanism used for video game joysticks.

One potential issue was the large size of our final model. One reason justifying our choice of size was to avoid the complications due to the roughness of PLA in FDM printing for a small model (especially for the ball joints). While its size also made it suitable for prototyping and demonstration purposes, downscaling the design would be necessary to serve industrial and practical purposes.

The implementation of our spherical rolling approximation method could have been further improved: unsuccessful communication of the mathematical results contained in this report led to erroneous implementation of the offset h_0 in the design. Thanks to our modular design, we swapped the necessary parts to include cable guides in fig. 8b which are more suitably offset from the centres of rotation of the links, although it was not optimal, as previously discussed.

In conclusion we believe we have successfully investigated the wrist mech-

anism of the quaternion wrist of LIMS2-AMBIDEX, considering our successful mathematical modelling, research and experimental design to create our own prototype of the model.

References

[1] R. Bischoff et al. "The KUKA-DLR lightweight robot arm—A new reference platform for robotics research and manufacturing". In: *Proc. 6th Ger. Conf. Robot.* (2010), p. 1.

[2] A. Bicchi and G. Tonietti. "Fast and "soft-arm" tactics [robot arm design]". In: *IEEE Robotics Automation Magazine* 11.2 (2004), pp. 22–33. DOI: 10.1109/MRA.2004.1310939.

[3] David V. Gealy et al. *Quasi-Direct Drive for Low-Cost Compliant Robotic Manipulation*. 2019. arXiv: 1904.03815 [cs.RO].

[4] Yong-Jae Kim. "Anthropomorphic Low-Inertia High-Stiffness Manipulator for High-Speed Safe Interaction". In: *IEEE Transactions on Robotics* 33.6 (2017), pp. 1358–1374. DOI: 10.1109/TRO.2017.2732354.

[5] Yong-Jae Kim, Jong-In Kim, and Wooseok Jang. "Quaternion Joint: Dexterous 3-DOF Joint Representing Quaternion Motion for High-Speed Safe Interaction". In: *2018 IEEE/RSJ International Conference on Intelligent Robots and Systems (IROS)* (2018), pp. 935–942. DOI: 10.1109/IROS.2018.8594301.

[6] Florian Petit et al. "Analysis and Synthesis of the Bidirectional Antagonistic Variable Stiffness Mechanism". In: *Mechatronics, IEEE/ASME Transactions on* PP (June 2014), pp. 1–12. DOI: 10.1109/TMECH.2014.2321428.